Journal of Luminescence 192 (2017) 728–733

Contents lists available at ScienceDirect

Journal of Luminescence

journal homepage: www.elsevier.com/locate/jlumin

Temperature dependence of white light emission and energy transfer in Dy^{3+} and Tm^{3+} co-doped $LiNbO_3$ single crystals

Siwei Long[a], Decai Ma[b], Yunzhong Zhu[b], MingMing Yang[a], Shaopeng Lin[b,*], Biao Wang[a,b,*]

[a] School of Physics and Engineering, Sun Yat-sen University, Guangzhou 510275, China
[b] Sino-French Institute of Nuclear Engineering and Technology, Sun Yat-sen University, Zhuhai 519082, China

ARTICLE INFO

Keywords:
Spectroscopic properties
Tm:Dy:CLN
White light emission
Energy transfer
Temperature dependence

ABSTRACT

The spectroscopic characteristics of the thulium and dysprosium co-doped congruent $LiNbO_3$ (Tm:Dy:CLN) single crystals have been studied for white-light generation. The chromaticity coordinates, color purity and color temperature could be tuned with different doping concentrations or temperatures. Optimal white emission was achieved when co-doped 0.5 mol% Tm^{3+} and 1.0 mol% Dy^{3+} under 363 nm excitation. The optimal operating temperature of Tm(0.5 mol%):Dy(1 mol%):CLN for white emissions was determined to be 400 K with the minimum color purity of 10%. The energy transfers between Tm^{3+} and Dy^{3+} were analyzed in detail and the energy transfer efficiencies at temperature ranging from 20 K to 430 K were determined. The results in this paper indicated the potential applications of Tm:Dy:CLN in optical temperature sensors and ultraviolet (UV) excited white light emission.

1. Introduction

In recent years, appreciable interest has been focused on the white light emitting diodes (W-LED) because of the promising advantages, such as long lifetime, high efficiency, high reliability, environment friendliness and so on. A new alternative trend to achieve white light emitting effectively consisted in combining the visible emitting light under UV excitation of rare-earth (RE^{3+}) ions, the energy levels of which cover a wide spectral range. To develop promising new all solid-state white emitting materials, much effort has concentrated on the RE^{3+} co-doped materials, including, for instance, the Tb^{3+}:Eu^{3+} [1], Dy^{3+}:Eu^{3+} [2], Eu^{2+}:Sm^{3+} [3], Er^{3+}:Tm^{3+} [4] and Tb^{3+}:Sm^{3+} [5,6] co-doped systems. Besides, the spectroscopic investigations on Ho^{3+}:Yb^{3+}:Tm^{3+} [7,8] tri-doped systems at room temperature have been reported and the potential application in multicolor display has been discussed. Among all the lanthanide ions, Dy^{3+} is distinguished for generating yellow light ($^4F_{9/2} \rightarrow {}^6H_{13/2}$) and blue light ($^4F_{9/2} \rightarrow {}^6H_{15/2}$) simultaneously. The yellow light intensity is sensitive to the host material and mostly dominant, on account of the peculiarity of the transition $^4F_{9/2} \rightarrow {}^6H_{13/2}$ [9]. With the intense blue emitting under ultraviolet excitation related to the transition $^1G_4 \rightarrow {}^3H_6$ of Tm^{3+} [10], Tm^{3+} could be chosen as codopant to adjust the color proportion for white light emitting.

In prior studies, glasses and ceramics are the most common host materials to obtain white light emission [11,12]. There are some inevitable drawbacks: low luminescent efficiency, inferior mechanical and thermal properties. As single-phased host materials, oxide single crystals show better mechanical and thermal performance and higher optical transmittance but were less adopted. Lithium niobate, one of the most widely used integrated optical materials, had been studied intensively and the spectroscopic properties of Dy^{3+} or Tm^{3+} doped Congruent $LiNbO_3$ (CLN) (molar ratio $[Li]/[Nb] = 0.946$) had been reported in Ref. [13,14]. With the excellent electro-optical properties, nonlinear optics properties, a large optical transmission spectra range, and high thermal stability [15–17], CLN could be a promising alternative as white-light host material.

There have been some reports on the structure and optical properties of the co-doped system Dy^{3+}:Tm^{3+}. The previous studies were mainly focused on the influence of RE^{3+} ions doping concentration [18–22], crystal structure [23,24] and excitation wavelength [25–28] on tunable luminescence. Besides of the investigation on multicolor-luminescence in Ho^{3+}:Yb^{3+}:Tm^{3+} tri-doped system [7], the temperature, another important factor on white-light emissions had been rarely addressed. The corresponding research should be of great scientific importance and might expand the applications. Except for the insufficient research on temperature dependence of white light emissions, especially in the co-doped system Dy^{3+}:Tm^{3+}, to our knowledge, there was few research paper involving the influence of temperature on energy transfer efficiency between rare earth dopants.

Therefore, in this paper, The luminescent properties in Tm:Dy:CLN

---

* Corresponding authors at: Sino-French Institute of Nuclear Engineering and Technology, Sun Yat-sen University, Zhuhai 519082, China
E-mail addresses: lshpeng@mail.sysu.edu.cn (S. Lin), wangbiao@mail.sysu.edu.cn (B. Wang).

http://dx.doi.org/10.1016/j.jlumin.2017.07.049
Received 9 April 2017; Received in revised form 10 June 2017; Accepted 26 July 2017

crystals with different Tm^{3+} concentration under different UV excitation wavelengths were studied in detail and the white light emission would be accomplished as a sum of blue and yellow light emissions. Energy transfer between Tm^{3+} and Dy^{3+} was observed and discussed at the temperature ranging from 20 K to 430 K. The influence of temperature on white light emission in Tm(0.5 mol%):Dy(1 mol%):CLN was investigated.

2. Experimental

Li_2CO_3, Nb_2O_5, Tm_2O_3 and Dy_2O_3 of high purity were fully mixed and calcined in the platinum crucible. The concentration of Dy^{3+} in melt was kept 1 mol%, while the concentration of Tm^{3+} in melt varied from 0 mol%, 0.1 mol%, 0.5 mol% to 1 mol%. Homogeneous Tm:Dy:CLN crystals of good quality were grown along the *c* axis in air by the Czochralski method. Wafers with the thickness of 2.5 mm were obtained by cutting the central part of crystals perpendicular to the *c* axis and then polished for further optical tests. The wafers with Tm^{3+} concentration from 0 mol%, 0.1 mol%, 0.5 mol% to 1 mol% were referred as DT-0, DT-1, DT-2 and DT-3 respectively thereinafter. Besides, a single-doped crystal Tm: CLN, prepared through the same method, was used as a reference and referred as T-#.

X-ray diffraction patterns from 20° to 90° were recorded using a D-MAX 2200 VPC X-Ray Diffractometer. The absorption spectra were measured in 350–850 nm wavelength region using a Lambda 950 UV–Vis–NIR Spectrophotometer at room temperature. The fluorescence excitation spectra, emission spectra and decay curves were acquired using an EDINBURGH FLSP980 Photoluminescence Spectrometer. The experimental temperature for fluorescence emission spectra and decay curves ranged from 20 K to 430 K.

3. Results and discussion

3.1. XRD patterns

The XRD patterns of the doped $LiNbO_3$ samples and the congruent $LiNbO_3$ (JCPDS 78-0251) were presented in Fig. 1. The strong diffraction peaks of the samples attributed to $LiNbO_3$ were marked with the indices of lattice planes, indicating no remarkable change in the lattice structure after doping with Dy^{3+} and Tm^{3+}.

3.2. Absorption and excitation spectra

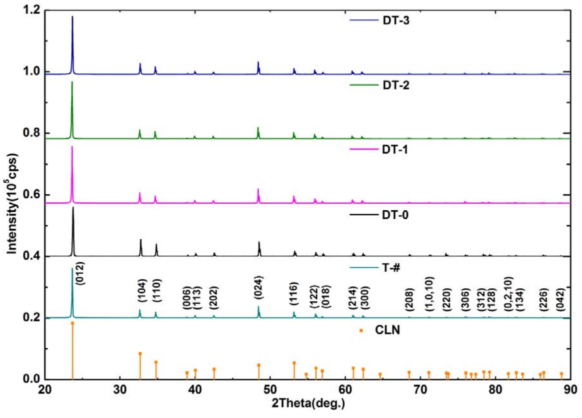

Fig. 1. The XRD patterns of the Tm^{3+} and Dy^{3+} single-doped and co-doped CLN crystals, and the un-doped CLN (JCPDS 78-0251).

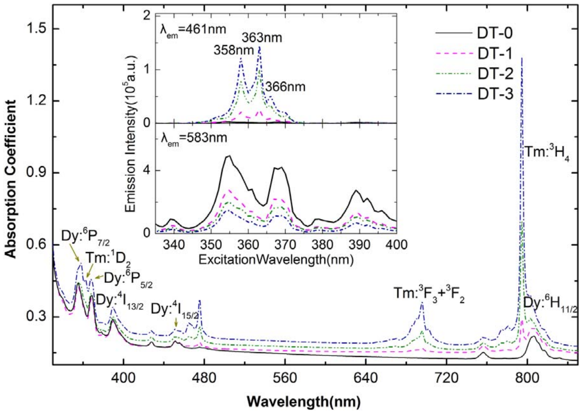

Fig. 2. The UV–VIS absorption spectra of the Tm:Dy:CLN wafers at room temperature in the 330–850 nm wavelength range. In the inset: the fluorescence excitation spectra with fixed emission wavelength at 461 nm and 583 nm.

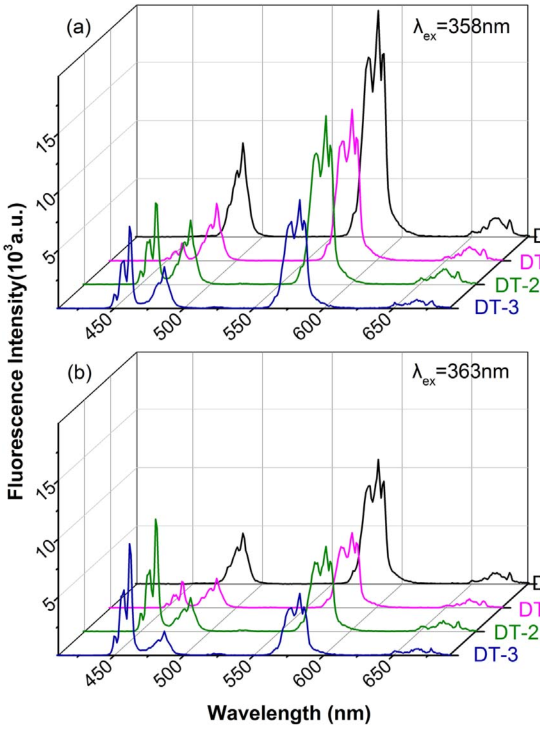

Fig. 3. The fluorescence emission spectra of Tm:Dy:CLN wafers under 358 nm and 363 nm excitation at room temperature.

Table 1
CIE chromaticity coordinates, color purity and color temperature (CCT) of Tm:Dy:CLN single crystals under 358 nm or 363 nm excitation.

λ_{ex}	Sample	CIE (x , y)	Color Purity (%)	CCT (K)
358	DT − 0	(0.4568,0.4408)	70	2970
	DT − 1	(0.4485,0.4273)	64	2995
	DT − 2	(0.3879,0.3558)	25	3618
	DT − 3	(0.3842,0.3443)	20	3608
363	DT − 0	(0.4555,0.4399)	69	2982
	DT − 1	(0.4228,0.3940)	46	3169
	DT − 2	(0.3401,0.2934)	16	4989
	DT − 3	(0.3196,0.2615)	25	6789

The UV–VIS absorption spectra of the Tm:Dy:CLN wafers in the 330–850 nm wavelength range were recorded at room temperature and presented in Fig. 2. The absorption bands related to the transitions from ground state to excited states (Dy^{3+}: $^6H_{15/2}$ to ^6H ^4I and ^6P terms, Tm^{3+}: $^3H_6$ to ^1D ^3F and ^3H terms) were marked up. The strong absorption around 800 nm, corresponding to transition $^6H_{15/2} \rightarrow {}^6F_{5/2}$ of Dy^{3+} and $^3H_6 \rightarrow {}^3H_4$ of Tm^{3+}, was commonly selected as excitation source for yellow emission. The UV Absorption bands centered at

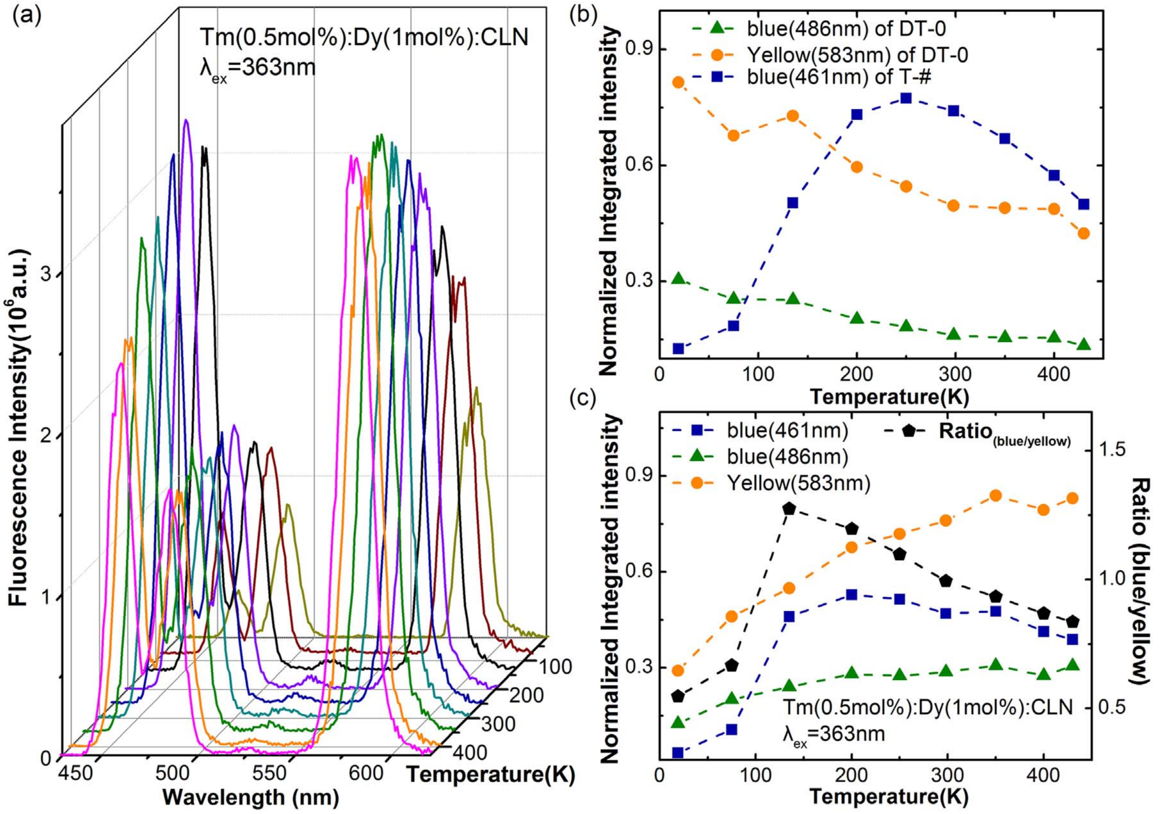

Fig. 4. (a) The fluorescence emission spectra of Tm(0.5 mol%):Dy(1 mol%):CLN (DT-2). (b) Normalized Integrated intensity variations of emission bands centered at 486 nm and 583 nm in Tm(0 mol%):Dy(1 mol%):CLN (DT-0), and 461 nm in Tm:CLN (T-#). (c) Left Vertical: Normalized Integrated intensity variations of emission bands centered at 461 nm, 486 nm and 583 nm in DT-2. Right Vertical: The integrated intensity ratio (blue/yellow) in the DT-2; the blue part of the ratio (blue/yellow) was determined as a sum of the emissions centered at 461 nm and 486 nm. The spectra, intensities and ratios above were obtained under 363 nm excitation with increased temperature from 20 K to 430 K. (For interpretation of the references to color in this figure legend, the reader is referred to the web version of this article.)

358 nm 363 nm 366 nm and 389 nm were attributed to the transitions: $^6H_{15/2} \rightarrow {}^6P_{7/2}$ (Dy^{3+}), $^3H_6 \rightarrow {}^1D_2$ (Tm^{3+}), $^6H_{15/2} \rightarrow {}^6P_{5/2}$(Dy^{3+}) and $^6H_{15/2} \rightarrow {}^4I_{13/2}$(Dy^{3+}) respectively. The excitation spectra of the Tm:Dy:CLN crystals with fixed emission wavelength at 461 nm and 583 nm were presented in the inset of Fig. 2. It was obvious that the yellow emissions centered at 583 nm would be dominant in visible region and intense blue emissions under 358 nm or 363 nm excitation were essential for optimal proportion to achieve the white light emitting.

3.3. Emission spectra with different Tm^{3+} concentration and white light generation

The fluorescence emission spectra of Tm:Dy:CLN wafers with various Tm^{3+} concentrations under 358 nm and 363 nm excitation was measured in 410–690 nm wavelength range and presented in Fig. 3. Intense yellow emissions centered at 583 nm (Dy^{3+}: $^4F_{9/2} \rightarrow {}^6H_{13/2}$), blue emissions centered at 486 nm (Dy^{3+}: $^4F_{9/2} \rightarrow {}^6H_{15/2}$) and relatively weak red emissions centered at 667 nm (Dy^{3+}: $^4F_{9/2} \rightarrow {}^6H_{11/2}$) were observed in all Tm:Dy:CLN samples. The blue emissions at 461 nm related to transition $^1D_2 \rightarrow {}^3F_4$ of Tm^{3+} were enhanced with the increased concentration of Tm^{3+} from 0 mol% to 1 mol%. The ratio of blue/yellow emission increased correspondingly. Besides, stronger blue emissions at 461 nm were obtained when excited at 363 nm than 358 nm, along with higher blue/yellow emission ratio. The CIE chromaticity coordinates and color temperature were calculated based on the fluorescence emission spectra and tabulated in Table 1. With the results, we concluded that white light emission could be accomplished in DT-2 and DT-3 under 363 nm excitation and 358 nm excitation respectively. The color purity was calculated using the formula [29]: $\sqrt{(x_s - x_i)^2 + (y_s - y_i)^2} / \sqrt{(x_d - x_i)^2 + (y_d - y_i)^2} \times 100\%$, where ($x_s$, y_s) (x_i, y_i) and (x_d, y_d) denote the CIE chromaticity coordinates of the samples, the standard white light ($x_i = 0.33$, $y_i = 0.33$) and the dominant wavelength. The results were added to Table 1. The color purity is 100% for pure color and 0% for standard white color. It is evident that the optical emission of Tm(0.5 mol%):Dy(1 mol%):CLN (DT-2) under 363 nm excitation was closer to the standard white light than others.

3.4. Energy transfer in Tm(0.5 mol%):Dy(1 mol%):CLN

The fluorescence spectra of Tm(0.5 mol%):Dy(1 mol%):CLN (DT-2) under 363 nm excitation, with which white light emission had been achieved above, were measured at temperature from 20 K to 430 K and presented in Fig. 4(a). The normalized integrated intensities ($\int I(\lambda)d\lambda$) of emission bands centered at 461 nm 486 nm and 583 nm in DT-2 were computed and presented in Fig. 4(c). The normalized integrated intensities of emission bands related to Dy^{3+}: yellow emission band centered at 583 nm (Dy^{3+}: $^4F_{9/2} \rightarrow {}^6H_{13/2}$) and blue emission band centered at 486 nm (Dy^{3+}: $^4F_{9/2} \rightarrow {}^6H_{15/2}$), increased as the temperature increased, while the normalized integrated intensity of the blue emission band centered at 461 nm related to the transition $^1D_2 \rightarrow {}^3F_4$ of Tm^{3+} increased with temperature ranging from 20 K to 200 K and then tended to decrease. In consequence, the corresponding integrated intensity ratio (blue/yellow), the blue part of which consisted of the emissions centered at 461 nm and 486 nm, was increased with increasing temperature from 20 K to 135K and then reduced with increased temperature above 135 K, as shown in Fig. 4(c).

As reported in Ref. [30] the thermal effect commonly lead to an increase of non-radiative relaxation and decrease the emission intensity as result, which was consistent with the temperature dependence of

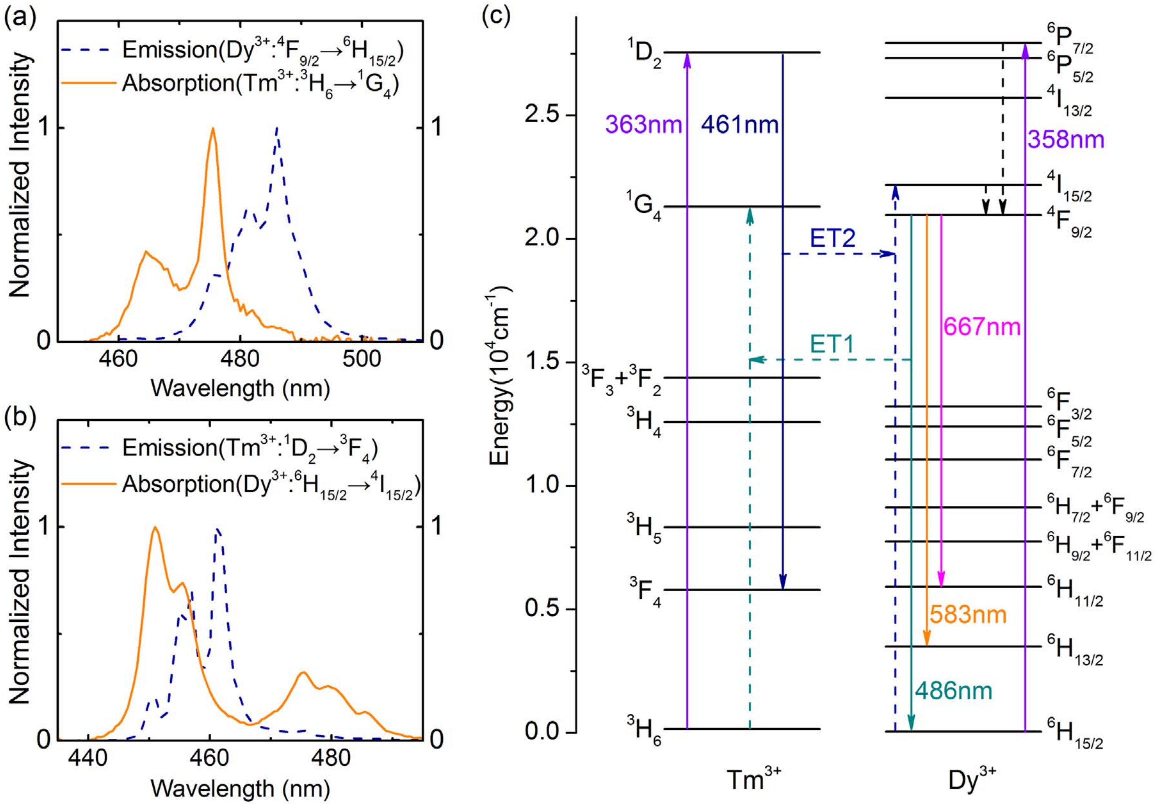

Fig. 5. (a) Overlap of Dy^{3+} emission band and Tm^{3+} absorption band in CLN. (b) Overlap of Tm^{3+} emission band and Dy^{3+} absorption band in CLN. (c) Energy level diagram of Tm (0.5 mol%):Dy(1 mol%):CLN, depicting the dominant energy transfer process and transition emission mechanism.

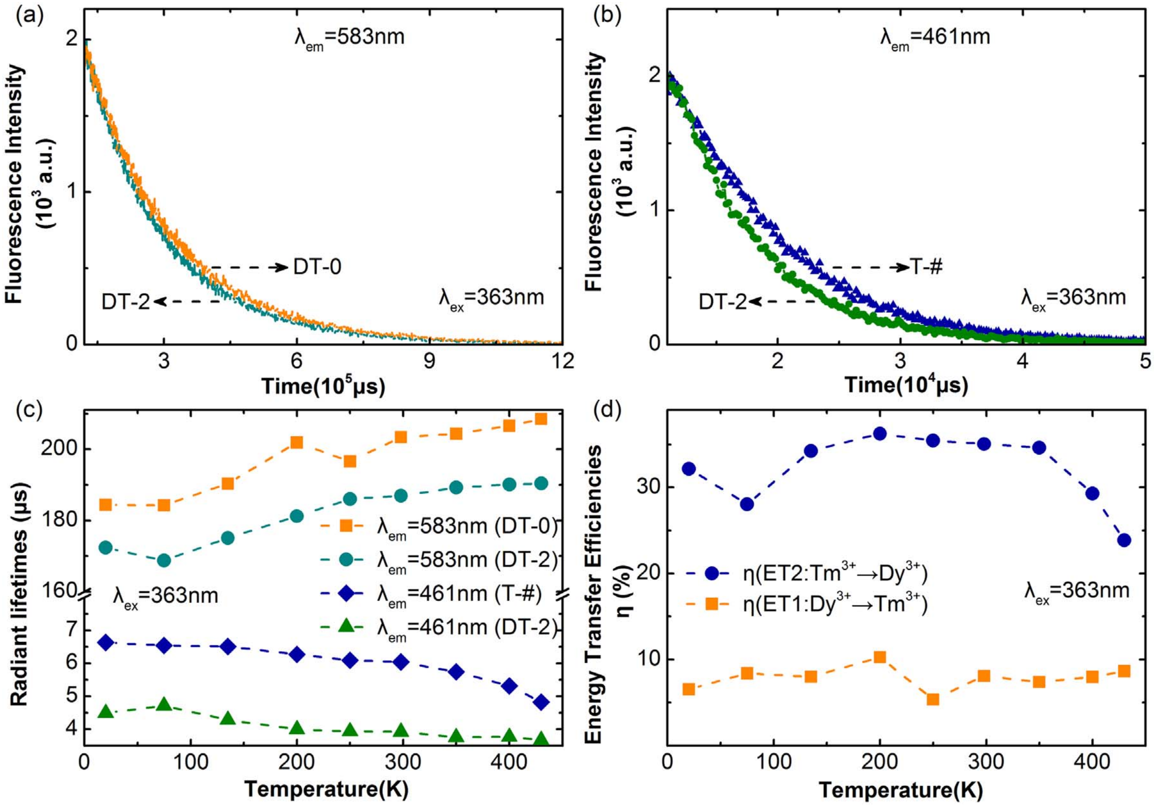

Fig. 6. The fluorescence decay curves of (a) the transition Dy: ${}^4F_{9/2}\rightarrow{}^6H_{13/2}$ (583 nm) or (b) the transition Tm:${}^1D_2\rightarrow{}^3F_4$ (461 nm) in Tm(0.5 mol%):Dy(1 mol%):CLN (DT-2), Tm:CLN (T-#) or Tm(0 mol%):Dy(1 mol%):CLN (DT-0) at 298 K. (c) The radiant lifetimes of the level Dy^{3+}:${}^4F_{9/2}$ in DT-0 or DT-2 and the radiant lifetimes of the level Tm^{3+}:${}^1D_2$ in T-# or DT-2 at temperature ranging from 20 K to 430 K. (d) The energy transfer efficiencies η_{ET1} ($Dy^{3+}\rightarrow Tm^{3+}$) and η_{ET2} ($Tm^{3+}\rightarrow Dy^{3+}$) at temperature from 20 K to 430 K.

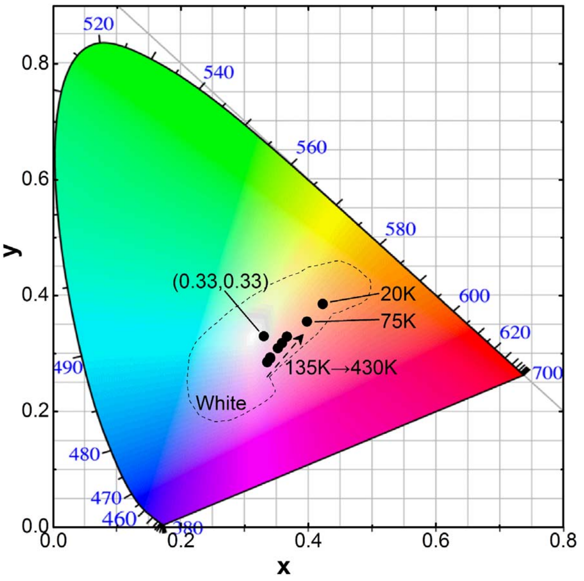

Fig. 7. The CIE chromaticity coordinates of white light emissions in the Tm(0.5 mol%):Dy (1 mol%):CLN single crystal under 363 nm excitation in the temperature range from 20 K to 430 K.

Table 2
CIE chromaticity coordinates, color purity and color temperature (CCT) of the Tm (0.5 mol%):Dy(1 mol%):CLN single crystal under 363 nm excitation in the temperature range from 20 to 430 K.

Temperature (K)	CIE (x , y)	Color Purity (%)	CCT (K)
20	(0.4225, 0.3857)	44	3103
75	(0.3978,0.3553)	27	3354
135	(0.3353,0.2852)	19	5267
200	(0.3356,0.2858)	18	5248
250	(0.3400,0.2915)	17	4984
298	(0.3401,0.2934)	16	4989
350	(0.3521,0.3092)	12	4456
400	(0.3586,0.3181)	10	4245
430	(0.3664,0.3293)	11	4043

486 nm-emission and 583 nm-emission integrated intensities in Tm (0 mol%):Dy(1 mol%):CLN (DT-0) presented in Fig. 4(b). Despite the common downward trend of experimental emission intensities of RE^{3+} especially at high temperatures, there could be sometimes an upward trend at a certain low temperature range in single-doped materials, the emissions of Nd:$LaAlO_3$ [31] and Dy:$65B_2O_3$-$30Na_2O$-5CaO [32] for example. In our experiment, the integrated intensity of 461 nm emission in Tm:CLN (T-#) increased first and then decreased at temperature higher than 250 K as shown in Fig. 4(b). The thermal characteristics might be one reason for the emission intensity variation of Tm^{3+} in the co-doped sample DT-2, but conflicted with the emission intensity variation of Dy^{3+} in DT-2: increasing with increased temperature until 350 K. The abnormal temperature-dependent emission intensity variation of Dy^{3+} in DT-2, which was unusual and similar to the emission variation of Tm^{3+} at 700 nm in the Ho^{3+}:Yb^{3+}:Tm^{3+} tri-doped $LiNbO_3$ [7], should be accounted for in terms of the energy transfer between Tm^{3+} and Dy^{3+} [33,34] after Tm^{3+} co-doping.

Since the probability of energy transfer is proportional to the overlap area between the absorption spectrum of the acceptor and the emission spectrum of the donor [33] according to Dexture's theory [35], with the significant overlap between the Tm^{3+} absorption band ($^3H_6 \rightarrow {}^1G_4$) and the Dy^{3+} emission band ($^4F_{9/2} \rightarrow {}^6H_{15/2}$) presented in Fig. 5(a), an energy transfer process from Dy^{3+} to Tm^{3+} (ET1) was confirmed. The fluorescence decay curves of the transition Dy^{3+}: $^4F_{9/2} \rightarrow {}^6H_{13/2}$ (583 nm) in DT-0 or DT-2 were measured at temperature from 20 K to 430 K and the curves obtained at 298 K were shown in Fig. 6(a). The radiant lifetimes of the level Dy^{3+}:$^4F_{9/2}$ in DT-0 and DT-2 at temperature ranging from 20 K to 430 K were determined and plotted in Fig. 6(c). The energy transfer efficiency ($\eta_{ET1} = 1 - \tau_{DT\text{-}2}/\tau_{DT\text{-}0}$) of ET1 plotted in Fig. 6(d) varied between 5.36% and 10.26% without regularity. With the relatively low value of η_{ET1}, the effect of ET1 on emission intensity was negligible.

There should be another energy transfer process from Tm^{3+} to Dy^{3+} (ET2), caused by the significant overlap of the Dy^{3+} absorption band ($^6H_{15/2} \rightarrow {}^4I_{15/2}$) and the Tm^{3+} emission band ($^1D_2 \rightarrow {}^3F_4$) presented in Fig. 5(b). The fluorescence decay curves of the transition Tm^{3+}:$^1D_2 \rightarrow {}^3F_4$ (461 nm) in T-# or DT-2 were measured at temperature from 20 K to 430 K and the curves obtained at 298 K were shown in Fig. 6(b). The radiant lifetimes of the level Tm^{3+}:$^1D_2$ in T-# and DT-2 were determined by single exponential fitting and double exponential fitting respectively and plotted in Fig. 6(c). The energy transfer efficiencies of ET2 ($\eta_{ET2} = 1 - \tau_{DT\text{-}2}/\tau_{T\text{-}\#}$) were calculated and added to Fig. 6(d). ET2 should be dominant, weakening the upward trend of emission intensities of Tm^{3+} in DT-2 at temperature from 20 K to 250 K, since η_{ET2} was remarkably greater than η_{ET1}. The increasing η_{ET2} at temperature ranging from 75 K to 200 K might be an important reason for the increasing emission intensity of Dy^{3+} in DT-2. When the operating temperature was above 200 K, η_{ET2} decreased with increasing temperature, which was consistent with the variation of Tm^{3+} emission. With the decreasing η_{ET2}, emission intensity of Dy^{3+} in DT-2 still kept increasing but started to flatten at 350 K.

To depict the dominant energy transfer process and emission mechanism of the Tm(0.5 mol%):Dy(1 mol%):CLN single crystal, The energy level diagram was presented in Fig. 5(c).

3.5. *The temperature-dependent white light in Tm(0.5 mol%):Dy(1 mol %):CLN*

The CIE chromaticity coordinates of Tm(0.5 mol%):Dy(1 mol %):CLN under 363 nm excitation with increased temperature from 20 K to 430 K were calculated and presented in the CIE chromaticity diagram, as shown in Fig. 7. The CIE chromaticity coordinates were within the white region consistently. At temperature range of 20–135 K, the CIE chromaticity coordinates moved from the yellow region (581 nm) to the blue region (461 nm), followed by a slow trend of shifting toward the yellow region with increased temperature from 135 K to 430 K. The temperature-dependent color tuning property apparently resulted from the variation of blue/yellow integrated intensity ratio and the energy transfer process. The corresponding color temperature and color purity were calculated and listed in Table 2. With the operating temperature exceeding (below) 135 K, there was a negative (positive) correlation between the color temperature and the operating temperature, which might find application in temperature measurement. The minimum of color purity was 10% at 400 K, indicating that the optimal operation temperature for white light generation in Tm(0.5 mol%):Dy(1 mol %):CLN was 400 K.

4. Conclusion

The luminescence properties of Tm^{3+} and Dy^{3+} single and co-doped CLN single crystals have been investigated over a wide range of temperatures. The chromaticity coordinates, color purity and color temperature of Tm:Dy:CLN crystals with various Tm^{3+} concentration under 358 nm and 363 nm excitation were determined. And the white light emission was accomplished in the Tm(0.5 mol%):Dy(1 mol%):CLN single crystal under 363 nm excitation. The energy transfer processes between Tm^{3+} and Dy^{3+} in Tm(0.5 mol%):Dy(1 mol%):CLN were analyzed at the temperatures ranging from 20 K to 430 K, indicating the energy transfer from Tm^{3+} to Dy^{3+} always dominant with higher efficiencies. Luminescence properties could be tuned with temperature and the optimal white light emission in Tm(0.5 mol%):Dy(1 mol %):CLN occurred at 400 K with the color purity of 10%. With the results, we proposed the potential applications of Tm:Dy:CLN in optical temperature sensors and UV-excited white light emission.

Acknowledgment

This project was supported by the NSFC (Nos. 11372361, 11302268, 10902128, 10732100, 50802026, 10972239), the Guangdong Science & Technology Project (2015B090927005) and the Fundamental Research Funds for the Central Universities (20174500031610022).

References

[1] S. Loos, F. Steudel, B. Ahrens, et al., Temperature-dependent luminescence and energy transfer properties of Tb^{3+} and Eu^{3+} doped barium borate glasses, J. Lumin. 181 (2017) 31–35.

[2] D. Rajesh, K. Brahmachary, Y.C. Ratnakaram, N. Kiran, A.P. Baker, G.G. Wang, Energy transfer based emission analysis of Dy^{3+}/Eu^{3+} co-doped ZANP glasses for white LED applications, J. Alloy. Compd. 646 (2015) 1096–1103.

[3] Z.G. Cui, R.G. Ye, D.G. Deng, Y.J. Hua, S.L. Zhao, G.H. Jia, C.X. Li, S.Q. Xu, Eu^{2+}/Sm^{3+} ions co-doped white light luminescence SrSiO$_3$ glass-ceramics phosphor for White LED, J. Alloy. Compd. 509 (2011) 3553–3558.

[4] X.L. Liang, S.L. Yuan, Y.X. Yang, G.R. Chen, The luminescence properties of Er^{3+}-doped and Er^{3+}-Tm^{3+}-co-doped phosphate glasses for white light emitting diode, J. Lumin. 130 (2010) 429–433.

[5] M.S. Kim, L.K. Bharat, J.S. Yu, White light emission characteristics of Tb^{3+} and Sm^{3+} co-doped CaYAlO$_4$ nanocrystalline phosphors for solid-state lighting, J. Lumin. 142 (2013) 92–95.

[6] Y. Il Jeon, L.K. Bharat, J.S. Yu, White-light emission of Ca$_2$La$_8$(GeO$_4$)$_6$O$_2$: Tb^{3+}/Sm^{3+} nanocrystalline phosphors for solid-state lighting applications, J. Lumin. 166 (2015) 93–100.

[7] L.L. Xing, Y.L. Xu, R. Wang, W. Xu, Influence of temperature on upconversion multicolor luminescence in Ho^{3+}/Yb^{3+}/Tm^{3+}-doped LiNbO$_3$ single crystal, Opt. Lett. 38 (2013) 2535–2537.

[8] V. Mahalingam, R. Naccache, F. Vetrone, J.A. Capobianco, Enhancing upconverted white light in Tm^{3+}/Yb^{3+}/Ho^{3+}-doped GdVO$_4$ nanocrystals via incorporation of Li^{+} ions, Opt. Express 20 (2012) 111–119.

[9] P.A. Ryabochkina, S.A. Antoshkina, E.V. Bolshakova, M.A. Ivanov, V.V. Kochurihin, A.V. Malov, S.N. Ushakov, N.V. Shchuchkina, K.N. Nishchev, Hypersensitive transitions of Tm^{3+}, Ho^{3+} and Dy^{3+} rare-earth ions in garnet crystals, J. Lumin. 132 (2012) 1900–1905.

[10] U. Hommerich, E.E. Nyein, D.S. Lee, A.J. Steckl, J.M. Zavada, Photoluminescence properties of *in situ* Tm-doped Al$_x$Ga$_{1-x}$N, Appl. Phys. Lett. 83 (2003) 4556–4558.

[11] M. Jayasimhadri, K. Jang, H.S. Lee, B.J. Chen, S.S. Yi, J.H. Jeong, White light generation from Dy^{3+}-doped ZnO-B$_2$O$_3$-P$_2$O$_5$ glasses, J. Appl. Phys. 106 (2009) 013105.

[12] G.H. Liu, Z.Z. Zhou, Y. Shi, Q. Liu, J.Q. Wan, Y.B. Pan, Ce:yag transparent ceramics for applications of high power LEDs: thickness effects and high temperature performance, Mater. Lett. 139 (2015) 480–482.

[13] P. Haro-Gonzalez, L.L. Martin, I.R. Martin, G.G. Dominiak-Dzik, W. Ryba-Romanowski, Pump and probe measurements of optical amplification at 584 nm in dysprosium doped lithium niobate crystal, Opt. Mater. 33 (2010) 196–199.

[14] E. Cantelar, G.A. Torchia, F. Cusso, Characterization of up-conversion processes in Tm^{3+}-doped LiNbO$_3$, J. Lumin. 122 (2007) 459–462.

[15] T. Zhang, B. Wang, S.Q. Fang, Y.Q. Zhao, F.R. Ling, Y.H. Xu, Investigation on the growth and structure of Fe-doped near-stoichiornetric LiNbO$_3$ crystal, J. Mater. Sci. 39 (2004) 5799–5801.

[16] T. Zhang, B. Wang, S.Q. Fang, D.C. Ma, Growth and photorefractive properties of an Fe-doped near-stoichiometric LiNbO$_3$ crystal, J. Phys. D: Appl. Phys. 38 (2005) 2013–2016.

[17] G.H. Lee, Optical properties of ZnO thin films on LiNbO$_3$ and LiTaO$_3$ substrates grown by pulsed laser deposition, Solid State Commun. 128 (2003) 351–354.

[18] G.V. Lokeswara Reddy, L. Rama Moorthy, P. Packiyaraj, B.C. Jamalaiah, Optical characterization of YAl$_3$(BO$_3$)$_4$:Dy^{3+}-Tm^{3+} phosphors under near UV excitation, Opt. Mater. 35 (2013) 2138–2145.

[19] Y. Li, X.C. Wang, W.J. Liu, C. Wang, Y.H. Wang, Photoluminescence properties and energy transfer of a color tunable phosphor: Dy^{3+} and Tm^{3+} co-activated SrCaAl$_2$SiO$_7$, Mater. Res. Bull. 76 (2016) 273–278.

[20] X. Sun, S.L. Zhao, Y. Fei, L.H. Huang, S.Q. Xu, Structure and optical properties of Dy^{3+}/Tm^{3+} co-doped oxyfluoride glass ceramics containing β-NaGdF$_4$ nanocrystals, Opt. Mater. 38 (2014) 92–96.

[21] P.H. Yang, X. Yu, X.H. Xu, T.M. Jiang, H.L. Yu, D.C. Zhou, Z.W. Yang, Z.G. Song, J.B. Qiu, Single-phased CaAl$_2$Si$_2$O$_8$:Tm^{3+}, Dy^{3+} white-light phosphors under ultraviolet excitation, J. Solid State Chem. 202 (2013) 143–148.

[22] W.Y. Zhao, S.L. An, B. Fan, S.B. Li, Tunable single-phased white-emitting phosphors Na$_3$YSi$_3$O$_9$:Tm^{3+}, Dy^{3+}, J. Lumin. 143 (2013) 71–74.

[23] X.L. Liang, C.F. Zhu, Y.X. Yang, S.L. Yuan, G.R. Chen, Luminescent properties of Dy^{3+}-doped and Dy^{3+}-Tm^{3+} co-doped phosphate glasses, J. Lumin. 128 (2008) 1162–1164.

[24] P.W. Zhou, Y.S. Zhu, W. Xu, L. Xu, H.W. Song, Controllable chrominance and highly improved luminescent quantum yield of YV$_{1-x}$P$_x$O$_4$:Tm, Dy, Eu inverse opal white light phosphors, Opt. Express 21 (2013) 25744–25751.

[25] L. Tang, H.P. Xia, P.Y. Wang, J.T. Peng, Y.P. Zhang, H.C. Jiang, Preparation and luminescence characteristics of LiYF$_4$:Tm^{3+}/Dy^{3+} single crystals for white-light LEDs, J. Mater. Sci. 48 (2013) 7518–7522.

[26] J.Y. Wang, J.B. Wang, P. Duan, Luminescence and energy transfer of Tm^{3+} or/and Dy^{3+} co-doped in Sr$_3$Y(PO$_4$)$_3$ phosphors with UV excitation for WLEDs, J. Lumin. 145 (2014) 1–5.

[27] Y. Lu, X.H. Tang, L.S. Yan, K.X. Li, X.M. Liu, M.M. Shang, C.X. Li, J. Lin, Synthesis and luminescent properties of GdNbO$_4$:re^{3+} (RE = Tm, Dy) nanocrystalline phosphors via the sol-gel process, J. Phys. Chem. C. 117 (2013) 21972–21980.

[28] A. Durairajan, D. Balaji, K.K. Rasu, S.M. Babu, Y. Hayakawa, M.A. Valente, Sol-gel synthesis and photoluminescence studies on colour tuneable Dy^{3+}/Tm^{3+} co-doped NaGd(WO$_4$)$_2$ phosphor for white light emission, J. Lumin. 157 (2015) 357–364.

[29] F.W. Mo, P.C. Chen, A.X. Guan, W. Zhang, L.Y. Zhou, Enhancement of luminescence intensity and color purity of Mg$_x$Zn$_1$-xMoO$_4$:Eu^{3+}, Bi^{3+} phosphors, J. Rare Earths 33 (2015) 1064–1071.

[30] D. Li, B.A. Dong, X. Bai, Y. Wang, H.W. Song, Influence of the TGA modification on upconversion luminescence of hexagonal-phase NaYF$_4$:Yb^{3+}, Er^{3+} nanoparticles, J. Phys. Chem. C. 114 (2010) 8219–8226.

[31] A. Bednarkiewicz, P.J. Deren, K. Lemanski, Anomalous decays in Nd^{3+} doped LaAlO$_3$ single crystal, J. Phys. Chem. Solids 85 (2015) 102–105.

[32] S. Tanabe, J. Kang, T. Hanada, N. Soga, Yellow/blue luminescences of Dy^{3+}-doped borate glasses and their anomalous temperature variations, J. Non-Cryst. Solids 239 (1998) 170–175.

[33] T. Sasikala, L.R. Moorthy, A.M. Babu, T.S. Rao, Effect of co-doping Tm^{3+} ions on the emission properties of Dy^{3+} ions in tellurite glasses, J. Solid State Chem. 203 (2013) 55–59.

[34] S.M. Liu, G.L. Zhao, X.H. Lin, H. Ying, J.B. Liu, J.X. Wang, G.R. Han, White luminescence of Tm-Dy ions co-doped aluminoborosilicate glasses under UV light excitation, J. Solid State Chem. 181 (2008) 2725–2730.

[35] D.L. Dexter, A theory of sensitized luminescence in solids, J. Chem. Phys. 21 (1953) 836–850.